Light-Activated Desorption of Photoactive Polyelectrolytes from Supported Lipid Bilayers

J. J. Benkoski,*,† A. Jesorka,† B. Kasemo,† and F. Höök‡

Department of Applied Physics, Chalmers University of Technology, Gothenburg, Sweden, and Solid State Physics Department, Lund University, Lund, Sweden

Received September 22, 2004; Revised Manuscript Received February 22, 2005

ABSTRACT: Phospholipid vesicles and supported bilayers have emerged as a promising platform for the development of biorecognition devices. To expand the capabilities of such biochips, it becomes desirable to direct and control the assembly of lipid structures into more sophisticated architectures. As one step toward this goal, we demonstrate the photoregulated desorption of a new class of polymer from lipid bilayers. The neutral, hydrophobic polymer resides within the bilayer under mild pH and ambient conditions. However, it contains side groups that can undergo excited state proton transfer (ESPT). The polymer therefore behaves as a polyelectrolyte when exposed to UV light. With the ensuing increase in hydrophilicity, the molecule is spontaneously ejected from the bilayer. Quartz crystal microbalance measurements with dissipation monitoring (QCM-D) have recorded this process and have shown that a rapid buffer exchange during light exposure results in efficient removal of the polymer from the system. Three polymers were tested in all: a polyanion, a polycation, and a polyzwitterion. A one-step approach to the synthesis of the monomer, performed under relatively mild reaction conditions, made it possible to synthesize each polymer in one step.

Introduction

Biochips. The biochip has much in common with the microprocessor, including batch processing, size, and design principles. Commercial biosensors already exist which are used clinically or for research and development.[1−3] Mostly owing to their miniaturization, they have improved the sensitivity, speed, and throughput of many biological tests.[4,5] In principle, the surface of a biosensor selectively binds to a biological analyte, which gives rise to a signal that is transferred into an electrical output through a signal transduction chain.[6] Such devices must also eliminate nonspecific binding to the surface in order to achieve the required sensitivity and specificity. In these cases the surface is typically modified with a probe molecule on or within a nonfouling polymer such as poly(ethylene glycol).[7,8] Alternatively, the host matrix can be supplied by a supported lipid bilayer.[9−12] Though not as robust as grafted polymer chains, supported lipid bilayers are even more biologically inert since they more closely mimic biological membranes.

Other advantages of supported lipid bilayers include the ability to host both water-soluble and transmembrane proteins. The hydrophobic nature of the membrane interior also opens up the possibility for novel anchoring principles. An interesting example has been reported with cholesterol-tagged DNA.[13] Since the coupling of probe molecules to the hydrophobic interior involves only noncovalent chemistry, it has several advantages over corresponding methods that involve functionalized lipids. These include faster coupling rates, removing the need for functionalized lipids, and eliminating unintended side reactions between the lipid functional groups and the other membrane constituents.[14]

A major disadvantage of supported lipid bilayers is that the coupling of biomolecules is difficult to control. This can be especially true in cases where the hydrophobic interior is used as the hosting matrix, since there are no obvious means to control the reversibility. The lack of reversible binding means that sensors of this kind can only be used once and that the analyte/probe complex, once formed, cannot be recovered. Reversibility is central for functions such as nanoscale separations and the ability to collect biomolecules for further processing.

In the current study we investigate a membrane-residing polymer that reversibly desorbs from lipid bilayers in response to a UV light stimulus. By coupling detector molecules to such a polymer, it may be possible to achieve the reversible anchoring of biological analytes to lipid-based biosensors.

Photoactive Polyelectrolyte. Figure 1 illustrates the mechanism by which a photoactive polyelectrolyte can reversibly desorb from a lipid bilayer in response to a light stimulus. A photoactive polyelectrolyte contains photoactive side groups, such as a photoacid, which form ion pairs when excited by light. At room temperature and physiological pH, the polymer chain is neutral and hydrophobic. It lowers the overall energy by embedding itself within the hydrophobic core of the bilayer. When the polymer is exposed to light at the absorption maximum, photoionization takes place, and the chain now behaves like a polyelectrolyte. The increased hydrophilicity leads to spontaneous ejection into the aqueous phase. If the photoionization involves only a proton exchange, then the polyelectrolyte rapidly returns to the neutral state upon removal of the light source.

Photoregulated binding to bilayer membranes has already been demonstrated for azobenzene-modified polyacrylates.[15,16] Ferritto et al. showed that the large increase in dipole moment that occurs after azobenzene is illuminated ($\lambda > 400$ nm) could be used to adjust the

† Chalmers University of Technology.
‡ Lund University.
* Corresponding author. E-mail: benkoski@fy.chalmers.se.

10.1021/ma048046q CCC: $30.25
Published on Web 04/06/2005

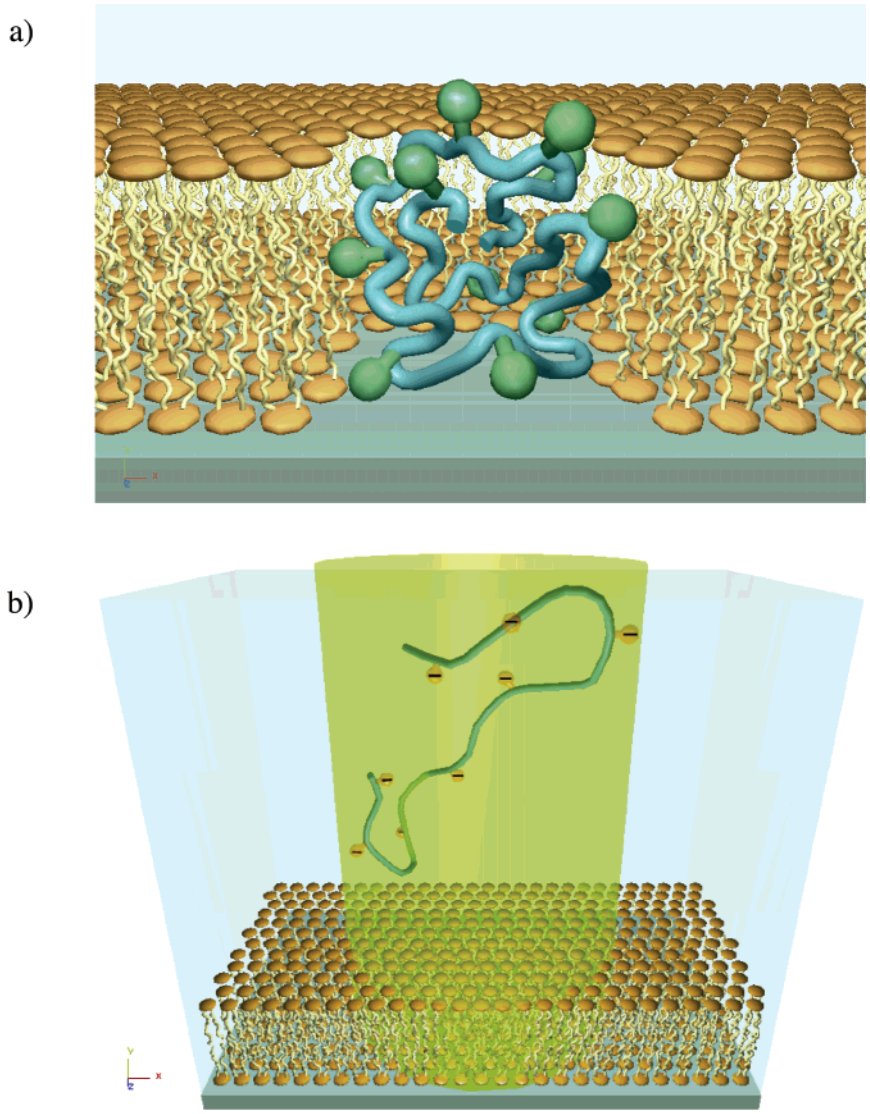

Figure 1. Schematic diagram of photoactive polyelectrolyte. (a) The polymer possesses neutral side groups and is hydrophobic. It lowers its energy by embedding itself within the hydrophobic core of the lipid bilayer. (b) The photoactive side groups ionize when exposed to UV light, making the polymer water-soluble and causing the release of the polymer into the aqueous phase.

degree of ionization of the polyelectrolyte. Although the apparent dissociation constant (pK_a) did not change greatly after light exposure, the increase in the degree of ionization of the light-adapted polymer was large between a pH of 6 and 7. The ensuing increase in solubility was sufficient for reducing the amount of vesicular binding as well as for decreasing the permeability of the membrane.

Excited-State Proton Transfer. The mechanism herein utilized to achieve reversible photoionization is referred to as excited-state proton transfer (ESPT). ESPT occurs when electronic excitation changes the acid−base properties of a molecule with respect to proton binding. Such behavior can occur when the molecule contains an N, O, or S heteroatom.[17] At these sites, the density of the lone electron pair increases or decreases, causing a change in the pK_a.

One such molecule that undergoes ESPT is 1-naphthol. At neutral pH in an aqueous medium, 1-naphthol exists in the neutral state. When exposed to light at a wavelength of 290 nm, its pK_a drops from 9.2 to 0.4.[18] It therefore undergoes rapid, reversible protolytic dissociation to furnish an anion in the excited state. 1-Naphthol has previously been used as a fluorescent probe in lipid membranes.[18,19] These studies utilized the strong tendency of this molecule to reside within the membrane interior. Sujatha et al. determined a binding energy of $-15k_BT$ for the neutral species in dimyristoylphosphatidylcholine (DMPC) liposomes at 30 °C.[20] A similar molecule, 2-naphthol, has been used by Gutman et al.[21,22] to modulate the pH of aqueous solutions with a laser pulse. Kinetic analysis of the pH jump indicated that ejection of the proton was completed within 100 ps, whereas the time constant for recombination with the proton was as high as 7 ms.

In addition to photoactive polyanions, the possibility also exists to use pendant groups that acquire a positive charge or make them zwitterionic. Quinoline, for example, has demonstrated enhanced basicity in the excited state. The pK_a of the quinolinium cation rises from 4.9 to 9.9 during UV light exposure.[23] Another related molecule is 8-hydroxyquinoline. A well-known chelating and fluorogenic reagent,[24] this molecule releases a proton from its hydroxy group and gains a proton on the nitrogen in the adjacent ring. The resulting tautomer is so stable that deprotonation occurs even in a solution of 10 M $HClO_4$.[25] From the above examples it can be seen that ESPT could potentially be used to

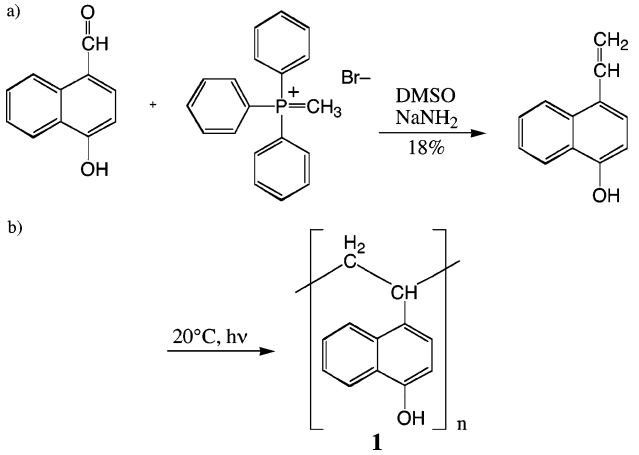

Figure 2. Schematic of (a) Wittig reaction used for monomer synthesis and (b) uncontrolled radical polymerization that occurs under ambient conditions.

tailor photoactive polyelectrolytes for many different applications.

Experimental Section

Monomer Preparation. Poly(4-vinyl-1-naphthol) (PVN, **1**) was synthesized in one step by a Wittig reaction. A schematic of the reaction is given in Figure 2. First, a stock solution containing 0.6 mM sodium amide and 0.6 mM methylphenylphosphonium bromide was prepared by diluting with anhydrous dimethyl sulfoxide (DMSO). To 2 mL of this solution was added 0.2 g (1.2 mmol) of 4-hydroxy-1-naphthaldehyde under nitrogen. After stirring 2 h at room temperature, the crude solids were precipitated in water. Silica gel chromatography with a 10:1 chloroform:methanol eluent was then used to recover the orange polymer in 18% yield.

The high reactivity of 4-vinyl-1-naphthol causes it to polymerize spontaneously under ambient conditions. The high molecular weight of the polymer could be observed by its ability to form tough films, and it could be measured using size exclusion chromatography (SEC). The structure of the polymer could also be confirmed using nuclear magnetic resonance spectroscopy (NMR). For the SEC measurements, the samples were eluted in trichlorobenzene at a temperature of 135 °C. The polymer obtained under these conditions had a number-average molecular weight (M_n) of 20.2 kg/mol with a polydispersity (PDI) of 2.2. Assuming a density of approximately 1 g/cm^3, the collapsed coil of this polymer would have a diameter of roughly 4 nm. This diameter compares with a typical lipid bilayer thickness of 4−5 nm.[26]

The Wittig reaction was repeated as above for both quinoline-4-carboxaldehyde and 8-hydroxyquinoline-2-carboxaldehyde. The resulting polymers, poly(4-vinylquinoline) (PVQ, **2**) and poly(2-vinyl-8-hydroxyquinoline) (PVHQ, **3**), were identified by their NMR spectra. The two polymers were synthesized with 59% and 66% yields, respectively. The molecular weights of these two polymers could not be determined accurately after many attempts due to complete loss of the samples in the GPC column. As is often the case with basic side groups, the nitrogen-bearing quinoline moieties interacted strongly with the oxidation present in the polystyrene columns. To circumvent this problem, viscosity measurements were performed for the three polymers in a glass capillary tube. Efflux times were recorded for five concentrations from 50 to 500 mg/mL in THF. Despite the limitations of the small sample sizes, the similar flow times suggested that the three viscosity-average molecular weights were roughly comparable.

Figure 3 gives a schematic representation of the photoionization process for the three polymers. In the case of PVN, the hydroxy group is deprotonated to form a polyanion. The N heteroatom in the quinoline ring of PVQ is protonated to form a polycation, and the 8-hydroxyquinoline ring of PVHQ is believed to tautomerize upon excitation to form a polyzwitterion. However, fluorescence spectrometry measurements for PVHQ described later cast some doubt on the picture given in Figure 3. As will be shown, these measurements suggest that either the OH group or N heteroatom form ions after the excitation of PVHQ, but possibly not both. All three ESPT reactions are expected to take place in water at a pH of 7.

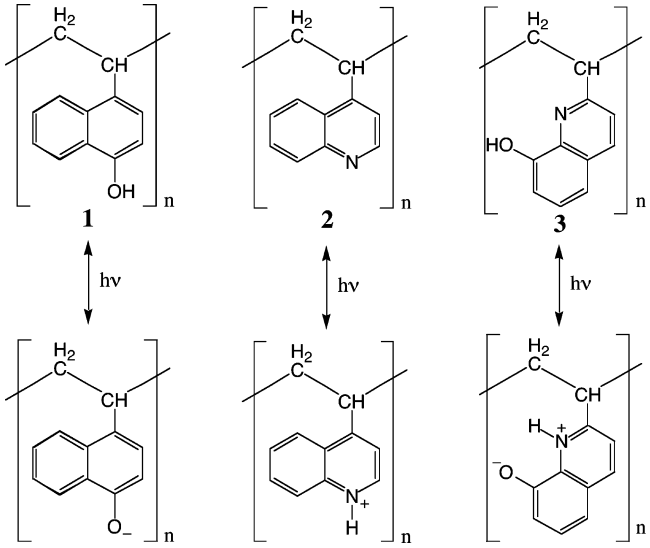

Figure 3. Schematic of photoionization process for all three photoactive polyelectrolytes. From left to right they are PVN **1**, PVQ **2**, and PVHQ **3**. Note that exposure to UV light causes a change from a neutral polymer to a polyanion, polycation, and polyzwitterion, respectively.

Cloud Point Measurements. The water solubility of the three polymers was tested by noting the pH at which an aqueous solution of the polymer became turbid. The polymers were first examined in pure water (Milli-Q, 18.2 MΩ) and were then tested in an electrolyte containing 10 mM TRIS and 100 mM NaCl. The solutions were prepared at a concentration of 0.5 mg/mL such that a change in the transparency of the mixture could be easily observed. All solutions were stirred vigorously with a magnetic stir bar, and the pH was adjusted by adding 0.1 M NaOH or HCl dropwise to the mixture.

Fluorescence Spectrometry. To verify that ESPT occurs when the polymers are exposed to UV light, fluorescence spectroscopy measurements were performed on each polymer. The spectra were obtained from a Spex Fluorolog 1681 0.22 m spectrometer (Horiba Jobin Yvon Inc.). Data acquisition was provided by the DataMax software package. The experiments were complicated by the fact that the polymers were insoluble in water (Milli-Q, 18.2 MΩ) at a pH of 7. In these cases, they were precipitated into a fine powder before mixing vigorously to form a 1 μM suspension (based on side-group concentration). PVN and PVHQ were excited at a wavelength of 315 nm, and the fluorescence emission was monitored from 325 to 600 nm. PVQ was excited at 305 nm, and its emission was monitored from 315 to 600 nm.

QCM-D. The quartz crystal microbalance (QCM) is based on a thin quartz crystal that is sandwiched between a pair of metal electrodes. An alternating electric field generated between these electrodes drives a piezoelectric response in the crystal. The ensuing oscillatory shear motion of the crystal occurs at a resonant frequency (f), which is determined primarily by the crystal's total mass. For a given added mass (Δm), there is a proportional change in the resonant frequency (Δf). This change increases linearly with overtone number (n = 1, 3, ...)[27]

$$\delta m_{\text{Sauerbrey}} = \delta_{\text{film}}\delta_{\text{film}} = \frac{C_{\text{QCM}}}{n}\delta_{\text{f}} \qquad (1)$$

where ρ_{film} is the effective density and δ_{film} is the effective thickness of the film. C_{QCM} is the mass sensitivity constant, measured to be 17.7 ng cm^{-2} Hz^{-1} for the crystals used in this

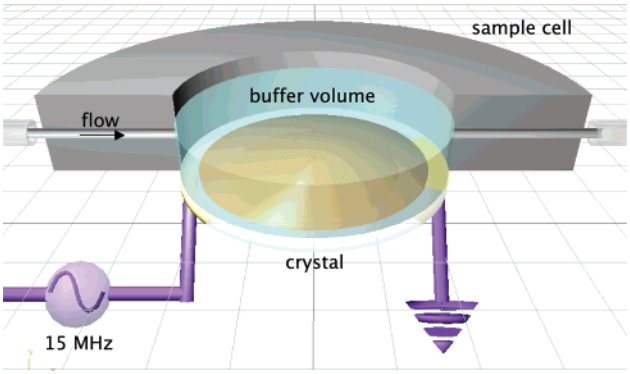

Figure 4. QCM schematic. The QCM crystal has two gold electrodes, one on each side. The top electrode is coated with a 300 nm thick layer of SiO_2. The alternating electric field established across the crystal generates an oscillating shear displacement along the plane of the crystal. The sample cell is designed for rapid buffer exchange from the tubes on either side. A quartz window on the top of the cell allows for UV light exposure.

study. One can detect mass changes below 10 ng/cm^2 using this relationship.[28] The sensitivity of this technique and its compatibility with aqueous environments have proven useful in the study of biological surface interactions.[29−34]

The above eq 1, known as the Sauerbrey relation, holds only if the adsorbed mass is small compared to the mass of the crystal, does not slip on the surface, and has negligible internal friction. However, even when these conditions are fulfilled, one must still use caution when converting Δf to Δm. In addition to mass changes, the resonant frequency also responds to changes in pressure, viscosity, temperature, and density of the aqueous medium. Water may also couple as additional mass via direct hydration, viscous drag, or entrapment within the film. The change in mass, therefore, typically includes both the adsorbed molecules and the coupled water.

Like other mechanical oscillators, quartz resonators lose energy while oscillating. The ratio of the energy lost to the energy stored per cycle is referred to as the dissipation factor (D).[35] When measured simultaneously with f, D can provide information about the viscoelastic properties of both the adsorbed film and adjacent medium (e.g., water). The inclusion of D has been shown to improve the interpretation of Δf in terms of mass uptake.[36]

Desorption Experiments. All QCM-D measurements were performed in a cell designed for fast exchange of a liquid (Q-Sense AB, Sweden). A schematic is given in Figure 4. At the top of the cell is a quartz window through which UV light can be shone on the sample. With a fundamental resonant frequency of 5 MHz, the AT-cut quartz crystals were coated with a 300 nm layer of SiO_2. They were driven into resonance at the first overtone (15 MHz), and the results were captured to a computer using the Q-Sense D 300 analysis equipment (Q-Sense AB, Sweden).

An Exfo Acticure light source delivered UV light at an intensity of 90 mW/cm^2. The spectrum of the high-pressure mercury lamp ranged from 250 to 600 nm, with an intensity of 36 mW/cm^2 at the excitation wavelength (315 nm). A relatively high intensity was preferred to maximize the fraction of the side groups in the excited state.

To test the concept of reversible desorption, UV light was shone on a supported lipid bilayer (palmitoyloleoylphosphatidylcholine, POPC) containing the photoactive polyelectrolyte. The illumination was performed both in stagnant buffer and in conjunction with a buffer rinse. These experiments were repeated for a bare crystal in air, a bare crystal in buffer, and a crystal coated with a pure POPC bilayer as a control.

A second set of QCM experiments was performed to determine the effects of pH changes on polymer desorption. After achieving a stable baseline, the lipid bilayer doped with 10 wt % polymer was exposed to a 10 mM TRIS, 100 mM NaCl buffer in a pH range where the polymer is soluble. For PVN, PVQ, and PVHQ, the pH was chosen to be 12, 2, and 12, respectively. (Note that the headgroup of phosphatidylcholine is only neutral in the pH range 3−10 and that the chosen pH values are also outside of the effective range of the TRIS buffer.[37,38])

Vesicle Formation. Lipid vesicles were prepared using a modified procedure based on the method of MacDonald et al.[39] The first step of the procedure was to dissolve 5 mg of POPC and 0.25 mg of PVN (5 wt %) in 1 mL of chloroform. Next, the solvent was evaporated under nitrogen to form a thin film along the walls of a round-bottom flask. 1 mL of a stock solution consisting of 100 mM NaCl and 10 mM tris(hydroxymethyl)aminomethane (TRIS) with a pH of 8 was then added to the flask, and the contents were stirred until dissolved. Finally, the mixture was passed 11 times through a lipid vesicle extruder (Avanti Polar Lipids, Inc.) to form small unilamellar vesicles (SUVs). A 100 nm filter in the extruder produced 110 nm vesicles with a polydispersity of 1.2. These results were checked using a BI-90 particle sizer (Brookhaven Instruments Corp.). The same process was repeated for PVQ and PVHQ.

AFM. The supported lipid bilayers were inspected using contact-mode atomic force microscopy (AFM). A Molecular Imaging Pico Scan AFM was operated in contact mode using a scan rate of 300 nm/s and a scan angle of 90°. The probe tip, consisting of silicon nitride, had a spring constant of 0.06 N/m (Digital Instruments). According to the method of Schneider et al.,[40] the imaging forces were calculated to be 2.7 nN when scanning the surface of the lipid bilayer and 5.4 nN when probing the surface of the underlying QCM crystal.

ATR-FTIR Spectroscopy. Further characterization of the POPC bilayers was carried out on a Bio-Rad FTS 6000 spectrometer (Bio-Rad Laboratories) equipped with an ATR accessory from Pike Technologies. Three spectra were collected in all: a pure POPC bilayer, a pure PVHQ film, and a POPC bilayer which was preimpregnated with 10 wt % PVHQ. For each spectrum, 50 scans were collected with a nominal resolution of 0.5 cm^{-1}. The corresponding ATR spectrum of the TRIS buffer was used as a reference.

For these experiments it was important to establish that the polymer was, in fact, incorporated into the POPC bilayer. The alternate possibility is that the polymer does not associate with the POPC during vesicle preparation but rather forms a mixed suspension of pure POPC vesicles and polymer precipitates. Unfortunately, either a uniform suspension of PVHQ-containing vesicles or a mixed suspension of vesicles and PVHQ precipitates could result in codeposition of POPC and PVHQ upon the ATR crystal. We therefore formed the bilayers upon a small section of a clean glass slide in a separate container. The bilayer-coated glass was then transferred directly to the ZnSe crystal, which was already immersed in TRIS buffer. The glass slide was then clamped gently to the ZnSe surface before collecting the data. Next, the spectrum for the pure PVHQ film immersed in water was obtained separately upon a Si crystal since it gave better results.

Results

ESPT and Fluorescence. The fluorescence emission spectra for the three polymers are given in Figure 5. These measurements demonstrate that light-induced ionization occurs in all three polymers. Each spectrum shows two distinct emission bands, one given by the neutral species and a red-shifted band given by the ionic species. The two PVN bands occur at 345 and 470 nm. These agree with the values of 350 and 450 nm reported for pure 1-naphthol in water at a pH of 7.[18] The above spectra can be compared to those for PVQ, which similarly exhibit two distinct bands.

The fluorescence spectra of PVHQ in Figure 5 are harder to interpret. The emission band at 345 nm most likely arises from the neutral 8-hydroxyquinoline moiety. However, the position of the ESPT species is more

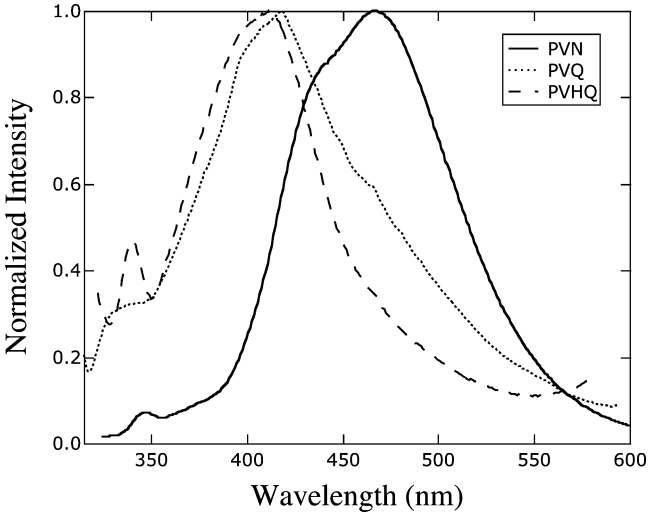

Figure 5. Fluorescence spectra for PVN (solid), PVQ (dotted), and PVHQ (dashed) suspended in water at a pH of 7. The fluorescence intensity has been normalized to the peak maximum. Each polymer displays two distinct peaks. In each case, the peak with the shorter wavelength is believed to arise from the neutral species, and the peak with the longer wavelength is believed to arise from the ionic species.

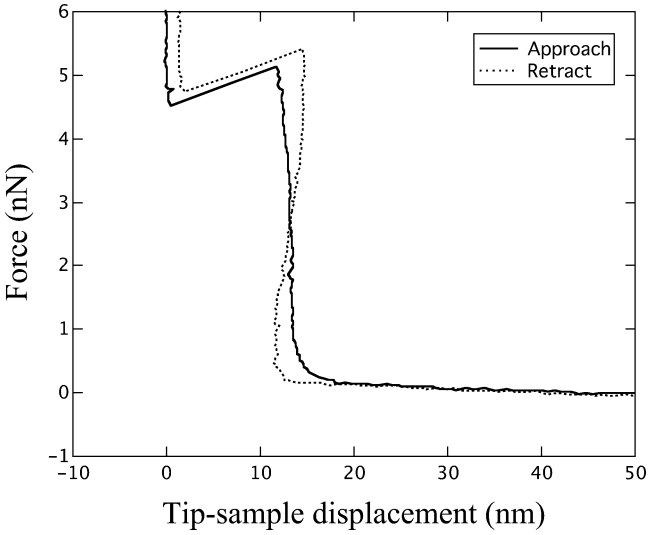

Figure 6. Force−displacement curve for the AFM tip. The discontinuity between 0 and 10 nm is due to the penetration of the AFM tip through the bilayer on the tip and the bilayer on the crystal surface. Surprisingly, the tip appears to jump out of contact at the same force during retraction.

consistent with the quinolinium cation, exhibiting a band at 410 nm. The expectation, in this case, is that the tautomer would fluoresce at a wavelength significantly higher than either 1-naphthoate or quinolinium. Bardez et al. found that the fluorescence spectrum of 6-hydroxyquinoline was dominated by the tautomeric peak at 580 nm.[25] Despite this discrepancy, a nearly identical spectrum was obtained for the starting material, 8-hydroxyquinoline-2-carboxaldehyde. The identity of the ionic species giving rise to the major band is therefore unclear.

Water Solubility. The cloud point of each polymer was measured to determine the appropriate pH ranges for conducting the desorption experiments. The results of these measurements indicate little difference in the pH of the cloud point whether purified water or 100 mM NaCl electrolyte was used. For both buffer and pure water, PVN is soluble above a pH of 9.7 ± 0.3, and PVQ is soluble below a pH of 2.9 ± 0.5. PVHQ is soluble both above a pH of 11.3 ± 0.2 and below a pH of 0. The latter value could not be determined precisely, however, for the cloud point occurred below the range of the pH electrode.

Bilayer Characterization. Bilayer formation was performed by immersing a UV ozone-treated[41] crystal into a 0.25 mg/mL POPC/polymer vesicle suspension. Since inclusion of the polymer inhibited bilayer formation, the original 5 mg/mL stock suspension was diluted to 0.25 mg/mL with a 10 mM TRIS buffer containing 100 mM $CaCl_2$.[42] $CaCl_2$ has been shown previously to induce bilayer formation for zwitterionic vesicles.[43]

The force−displacement profile of the AFM tip in Figure 6 indicates the presence of the bilayer by the discontinuity between 0 and 10 nm.[40,44] Since bilayers are typically about 5 nm thick,[26] the 10 nm jump likely indicates that both the crystal surface and the AFM tip are coated with a bilayer. The discontinuity, then, occurs when the AFM tip pierces through both bilayers above a critical force, approximately 5 nN in this case.[44] Surprisingly, the tip appears to jump out of contact at the same force during retraction. The unusual shape of the profile is believed to result either from the polymer embedded within bilayer or from the unusually high concentration of Ca^{2+}. Normally, one would expect the AFM tip to remain in contact with the surface until significant tension has developed. This adhesion arises due to van der Waals forces between the tip and substrate. Under the current conditions, the bilayer on the substrate rapidly pinches off from the bilayer on the AFM tip while the load is still compressive. The role of the polymer or Ca^{2+} is unclear, but one of them appears to resist the fusion of these two bilayers.

The thickness of the bilayer, measured to be approximately 4.6 nm, was determined from the step height of an incomplete bilayer (not shown). When using an imaging force of 2.7 nN, the surface image of the lipid bilayer revealed no discernible surface features. Likewise, the image of the underlying crystal surface obtained at an imaging force of 5.4 nN did not indicate the presence of polymer adsorbed to the crystal. Both images were essentially identical to that of the crystal before bilayer formation.

Since each "snapshot" of the surface can take up to 10 min to process, it is unable to image surface features whose mobility is large compared to the capture time. The AFM tip may also modify the surface topology either by pushing molecules along the surface or by deforming them with its downward force. As such, the lack of height contrast on the surface does not necessarily indicate the absence of the polymer; rather, the inability to image the embedded polymer chains should be interpreted as being due to their mobility, small size, or deformability.

Figure 7 is a typical QCM-D plot depicting bilayer formation. This particular plot is for 100 nm vesicles with 5 wt % PVHQ. Note the characteristic increase in dissipation and decrease in frequency. Such behavior is consistent with the formation of supported lipid bilayers.[45,46] Although the frequency drop is larger than that expected for a pure POPC bilayer (~ -77 Hz), it is possible that the embedded polymer either extends beyond the top of the bilayer or couples additional water. The higher than normal dissipation also supports this interpretation.[47]

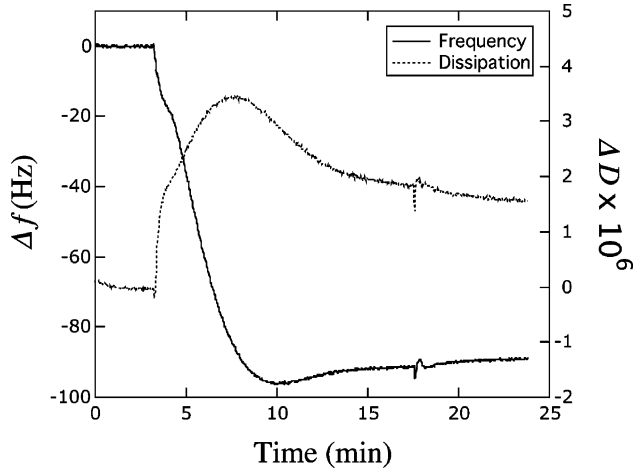

Figure 7. Formation of a POPC bilayer doped with 5 wt % PVHQ. The use of 100 mM $CaCl_2$ in the buffer truncates the depth of the frequency minimum compared to standard NaCl buffers.[43] The presence of the embedded polymer hindered bilayer formation and necessitated the use of multivalent counterions.

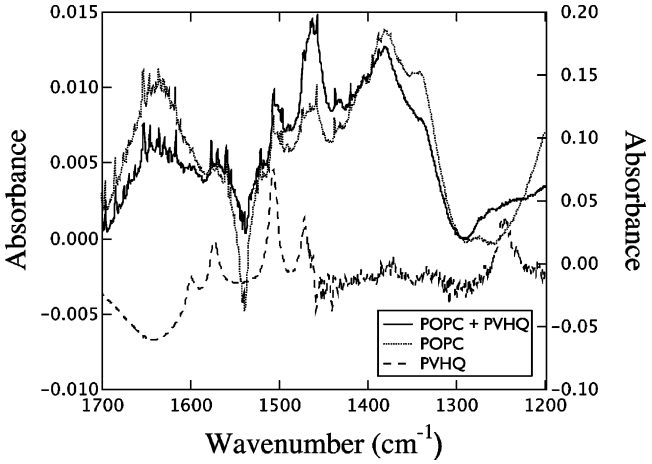

Figure 8. ATR-FTIR data for a pure PVHQ film immersed in buffer (dashed), a pure POPC bilayer (dotted), and a POPC bilayer preimpregnated with 10 wt % PVHQ (solid). Both lipid bilayers were formed upon glass slide sections in separate containers in order to rule out the possibility that PVHQ precipitates could deposit directly upon the ATR crystal. Note that the POPC + PVHQ spectrum exhibits stronger absorption than a pure POPC bilayer at each wavenumber where the pure PVHQ film exhibits a strong absorption.

ATR-FTIR Data. The FTIR data in Figure 8 include the spectra for a pure POPC bilayer, a POPC bilayer with 10 wt % PVHQ, and a thin film of PVHQ immersed in buffer. The latter spectrum is plotted against the secondary axis since it was a thicker film and exhibited a much larger absorbance than either bilayer. The data are obscured somewhat by the large absorption due to water near 1600 cm^{-1}. Note that this absorption is sensitive to small changes in the area of the glass slide or to the thickness of the adsorbed film. Also, note that many of the small peaks that appear as noise in the range from 1900 to 1500 cm^{-1} actually result from the rotational modes of gaseous H_2O in the sample chamber.

Within the range of 1700−1200 cm^{-1}, the pure PVHQ can be characterized by five peaks. These appear at 1600, 1575, 1505, 1475, and 1250 cm^{-1}. With the exception of the absorptions at 1600 and 1250 cm^{-1}, these peaks tend to overlap with the CH_2-CH_2 and $O-CH_2$ bending modes that appear in the POPC spectrum. Observe, however, that the POPC bilayer with 10 wt % PVHQ exhibits stronger absorption at each wavenumber where a strong PVHQ absorption exists. One may also note that the POPC + PVHQ spectrum appears to absorb at 1600 and 1250 cm^{-1} even though no corresponding peak is discernible in the pure POPC data. Given that 10% of a monolayer is difficult to detect, the ATR-FTIR spectra appear to indicate the incorporation of the polymer into the bilayer.

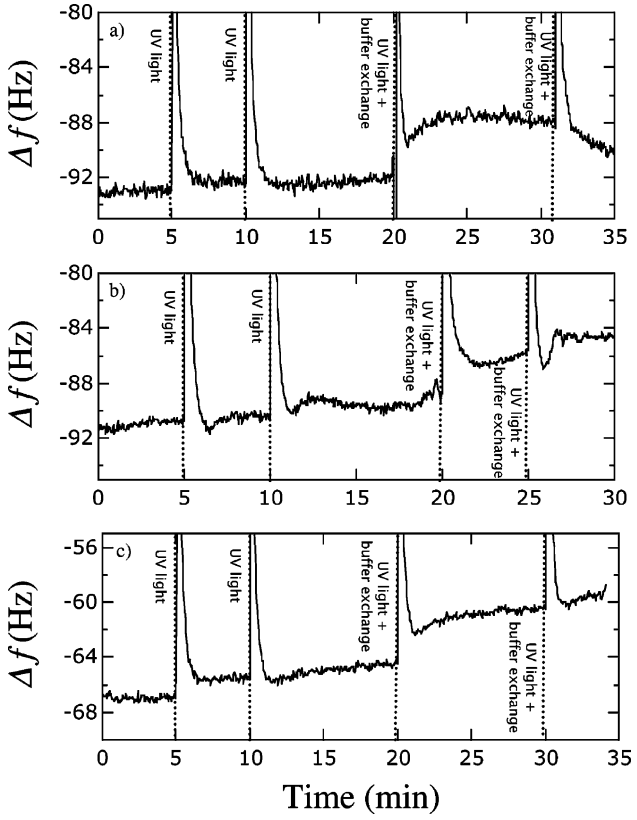

Figure 9. QCM-D spectrum for a POPC bilayer impregnated with (a) 5 wt % PVN, (b) 5 wt % PVQ, and (c) 5 wt % PVHQ. No significant change in baseline is generally observed for the first two peaks, which arise from 10 s light exposures. The second two exposures are performed in conjunction with a buffer exchange. Observe in each case that the frequency increases by approximately 5 Hz during the first buffer exchange/light exposure. This frequency increase corresponds roughly to a 5% loss in mass. No additional mass is lost when the buffer exchange/light exposure is performed the second time.

Desorption Experiments. The effect of UV light exposure on a POPC bilayer doped with 5 wt % PVN is given in Figure 9a. Notice that the 10 s exposure results in a rapid increase in QCM frequency. This frequency spike is believed to arise from bending stresses within the quartz, gold, and silica layers of the QCM sensor. Since each material absorbs different amounts of light, they are expected to change in temperature with respect to each other and, hence, generate a thermal expansion mismatch.

With regards to desorption of the polymer, the large transients make it difficult to assess the time evolution of surface reactions during the light exposure. The analysis is therefore limited to end-point measurements before and after each exposure. Accordingly, no permanent change in the frequency baseline is observed when a 10 s light exposure is performed in stagnant buffer (first two Δf spikes). A return to the baseline was not observed, however, when the light exposure was per-

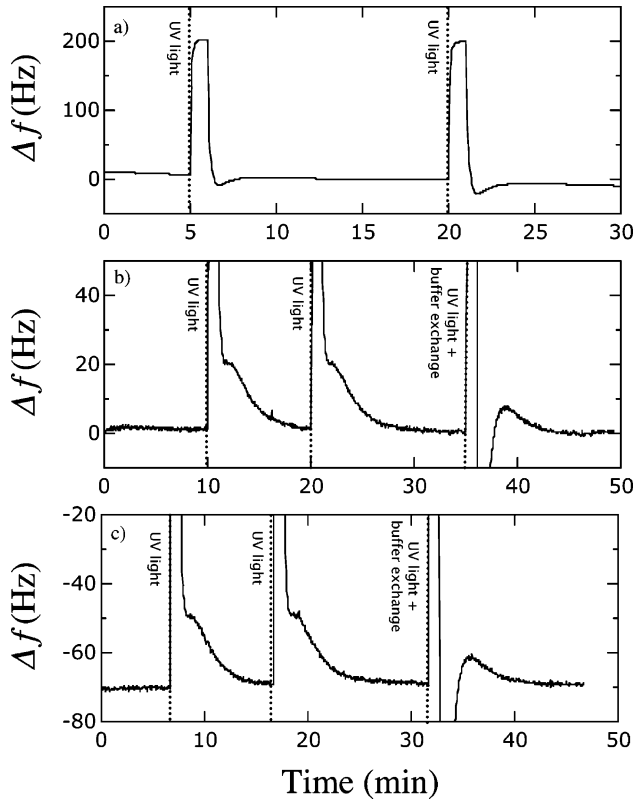

Figure 10. QCM-D data for (a) a bare quartz crystal in air, (b) a bare quartz crystal in buffer, and (c) a supported POPC bilayer in buffer. The peaks result from 60 s exposures to UV light at an intensity of 90 mW/cm^2. The third exposure in (b) and (c) was performed simultaneously with a buffer rinse. The flow rate was increased to nearly 3 times the normal rate for these experiments.

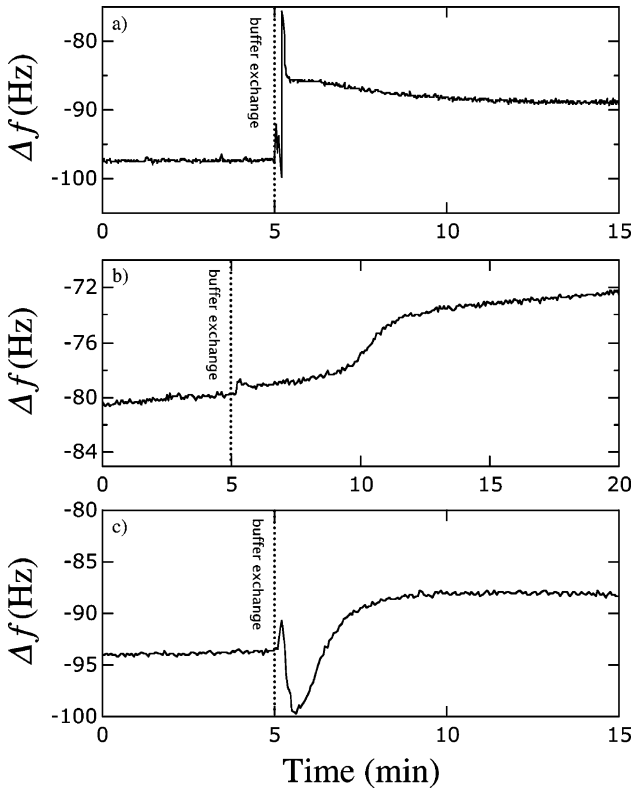

Figure 11. QCM-D results from the exposure of a POPC bilayer impregnated with (a) 10 wt % PVN to buffer with a pH of 12, (b) 10 wt % PVQ with a pH of 2, and (c) 10 wt % PVHQ with a pH of 12. The buffer exchange, shown by the small transient, is performed at 5 min. The increase in f after the buffer exchange ranges from 6 to 8 Hz. These changes correspond roughly to a 9% loss in mass for PVN, a 9% loss in mass for PVQ, and a 6% loss in mass for PVHQ.

formed simultaneously with a buffer exchange (third spike). The overall increase in the baseline frequency was approximately 5 Hz. This change corresponds to a 5 wt % loss in mass, coinciding with the amount of polymer embedded in the bilayer. Observe that a fourth exposure to UV light with a buffer exchange (fourth spike) did not result in the loss of additional mass. Although it is not known to what extent the baseline change includes the effects of coupled water, small changes in temperature, or hysteresis, the 5 Hz increase is consistent with complete removal of the polymer.

Figure 9b shows the same test performed for PVQ. It indicates that the majority of the polymer remains in the bilayer after light exposure (first two spikes). The removal of this polymer with a buffer exchange appears to be slightly less efficient, however. Only 4 wt % (4 Hz increase) of the bilayer is removed after the first buffer exchange (third spike). This value increases to 5 wt % (5 Hz increase total) after the second buffer rinse and light exposure (fourth spike). The results for PVHQ, shown in Figure 9c, are similar to the PVN results.

The control experiment performed on a bare QCM crystal is shown in Figure 10a. Here the exposure time has been increased to 60 s, and the buffer flow has been increased to nearly 3 times the normal rate in order to demonstrate that large transients do not cause permanent changes in the baseline frequency. Similar behavior is observed in Figure 10b, when the crystal is immersed in buffer. Here, the first two exposures are performed in stagnant buffer. The third exposure, performed in conjunction with a buffer exchange, also did not affect the baseline. Identical to this behavior is that found for a crystal coated with a pure POPC bilayer, shown in Figure 10c. These control experiments therefore demonstrate that UV light exposure does not cause a permanent change in frequency that might be mistakenly interpreted as a change in mass.

For the second set of QCM-D experiments, pH changes were used instead of light to induce polymer desorption. Figure 11a displays the results of exposing a POPC bilayer impregnated with 10 wt % PVN to a 100 mM NaCl buffer with a pH of 12. A 9 Hz increase in frequency (9 wt %) is observed. Figure 11b displays the effects of exposing a 10 wt % PVQ bilayer to a buffer with a pH of 2. Observe that 9 wt % (7 Hz increase) of the polymer desorbs from the bilayer but that this process does not begin until approximately 3 min after the buffer exchange. Finally, Figure 11c shows the desorption of PVHQ after exposure to buffer with a pH of 12. In this case only 6 wt % (6 Hz increase) is removed. This reduced efficiency is believed to result from the fact that the pH (12) is so close to the cloud point for this polymer (pH 11.3).

Discussion

Regulated Desorption. What we have demonstrated is the light-regulated desorption of photoactive polyelectrolytes from supported lipid bilayers. In the presence of UV light and buffer flow, the polymers can be efficiently removed from the system. We have also demonstrated the removal of the polymer in response to pH. Such control over the incorporation of molecules into the interior of lipid bilayers opens up the door not

only for innovative anchoring strategies but also for controlling the properties of the membrane itself.

As illustrated by the pH-controlled desorption of PVN, the process appears fairly straightforward. With increasing pH, the polymer becomes increasingly charged. Since the chemical potential for an ionized chain segment is lower in the aqueous phase, such segments most likely remain in contact with, or perform excursions into, the nearby water. This process progresses until the entire polymer chain is expelled from the bilayer. The soluble polymer then diffuses away from the interface.

Similar behavior would be expected for the combined UV light exposure and buffer exchange. However, this picture is complicated by is the apparent reversibility of the polymer desorption shown in Figure 9. For the first two light exposures, the illumination is performed in stagnant buffer. The recovery of the frequency baseline occurs in approximately 60 s, indicating that 100% of the polymer remains in the bilayer after the exposure. This observation can be explained by only two possibilities: either the polymer never desorbs during illumination, or the polymer desorbs during illumination but then completely returns to its original position in the bilayer within 60 s.

Since bilayers have such high resistance to the spontaneous adsorption of water-soluble macromolecules, the task of reincorporating the polymer into the bilayer is not trivial. A polymer chain, or any other hydrophobic particle, must first breach the outer layer of polar headgroups before embedding itself within the hydrophobic interior. Added to this hurdle is the relatively low concentration of polymer in the buffer once it is released.

Several factors may help to overcome these barriers. The first arises from the constraint placed on the lipid bilayer by the underlying substrate. Lacking the ability to contract, the bilayer likely remains in tension or creates defects after it loses 5% of its mass. Such strain or voids may make the inclusion of hydrophobic molecules more energetically favorable. They may also create easier pathways for the penetration of the polymer chains through the outer layer of the membrane. Also, facilitating incorporation is the geometry of the polymer. Unlike globular proteins, the polymers used in this study are not confined to a single conformation. They are able to change shape and may be somewhat flexible due to swelling with water. The ability to explore different conformations might therefore allow the polymer to lower the energy barrier of penetration by proceeding along a more favorable activation path.

The second alternative is that the polymer never completely disengages from the bilayer during light exposure. Although the ability to rinse away the polymer during illumination points to significant changes in solubility, one must be able to explain why the polymer can return to the bilayer so quickly. Here one can calculate the diffusion coefficient needed for this to occur. The distance traveled by the polymer in 10 s can be calculated by the familiar equation

$$x = \sqrt{2D_f t} \tag{2}$$

where D_f is the diffusion coefficient and t is the elapsed time of the light exposure. The expectation time for capture by the surface ($W(t)$) is given by[48]

$$W(t) = (2bx - x^2)/2D_f \tag{3}$$

where b is the linear dimension of the aqueous environment normal to the surface (size of the sample chamber). Substituting eq 2 into eq 3 gives

$$D_f = 2t\left(\frac{b}{W(t) + t}\right)^{-2} \tag{4}$$

Given that $b = 4$ mm, $t = 10$ s, and that $W(t) < 60$ s, the diffusion coefficient must be $>6.5 \times 10^{-4}$ cm^2/s. This value is about 1 order of magnitude higher than the self-diffusion coefficient of water at room temperature.[49] This result means that recapture of the polymer chains is not probable under these experimental conditions. The probability becomes even lower when one considers that the expectation time is defined when only 50% of the polymer has returned.

What should be noted about this analysis is that polyelectrolytes are generally known to complex with vesicles and bilayers. Seki and Tirrell found that poly(2-ethacrylic acid) (PEAA) adsorbed to L-α-dipalmitoylphaphatidylcholine vesicles up to a pH of 7.4.[50] At this pH, only 1% of the PEAA side groups are protonated.[51] This finding suggests that even highly charged polyelectrolytes can have an affinity for bilayer surfaces. The consequence of this result is that the polymers used in this study may not be entirely disengaged from the lipid bilayer during the 90 mW/cm^2 light exposure. Most likely the polymer exists in a state where the photoionized units are in contact with water, while the neutral units are shielded from water either by neighboring units or by lipids.

Recall that neutral 1-naphthol binds to DMPC liposomes with a binding energy of $-15k_BT$.[20] Even a few neutral moieties may therefore be sufficient to prevent complete desorption of the polymer. Perhaps, then, the increased perturbations resulting from the fluid flow are necessary to completely separate the polymer from the bilayer. Future studies will be needed to determine the degree of ionization as a function of light intensity and whether desorption can be induced in stagnant buffer at higher intensities.

In the case of the pH experiments, the pH adjustment was large enough to ensure complete ionization of the polymer. The fact that the polymer desorbed from the bilayer without any assistance from fluid flow indicates that the fully ionized polymer will spontaneously partition into the aqueous phase. This finding therefore suggests that photoionization of the polymer was incomplete in the UV experiments since light exposure alone did not produce the same result. Conversely, these observations also imply that spontaneous desorption can be induced solely by UV light at higher intensities.

Polymer Comparison. Although the QCM-D results for the three polymers were largely the same, their varied responses to pH should not be discounted. For light-induced desorption to occur, the pH of the medium should lie between pK_a and pK_a*. Only in the case of PVQ was the pH (8) close to the pK_a* (10). Not surprisingly, the removal of this polymer via combined light exposure/buffer exchange proved to be the least efficient of the three polymers.

The ability of PVHQ to desorb in response to UV light was also encouraging. The extreme pH values needed to dissolve this polymer suggested that such behavior was unlikely. However, the cloud point measurements

do not specify the efficiency with which the molecule can photoionize. This response depends on several factors, including the fluorescence lifetime and the rates of protonation and deprotonation. Fast deprotonation and slow reprotonation may therefore lead to higher degrees of ionization for a given light input.

Conclusions

We have demonstrated the light-controlled desorption of photoactive polymers from lipid bilayers. By stimulating the photoionization of the side groups, UV light exposure increased the water solubility of three classes of polymer: a polyanion, a polycation, and a polyzwitterion. Once soluble, the polymers could be efficiently removed from the system by performing the light exposure in conjunction with a buffer exchange. The polymer most likely did not become completely detached from the bilayer during light exposure in stagnant buffer because the diffusion rates are not sufficient for the polymer to diffuse away and then return to the bilayer within the amount of time indicated by the QCM data.

The relatively facile synthesis of these polymers also shows promise for the study of similar molecules. Many naphthalene-based molecules exist and offer the potential for precise tailoring of their properties toward specific applications. The synthesis also makes it possible to couple such polymers to various biomolecules for the purpose of developing biosensors with reversible adsorption capabilities.

Acknowledgment. J.J.B. thanks the N.S.F. for providing him with the MPS/DRF Distinguished International Postdoctoral Fellowship under Award DMR-0301195. He also thanks Krystina Brzezinska for her helpful discussions regarding chemistry, Johan Hurtig for help with fluorescence microscopy, Ansgar Willie for help with ATR-FTIR measurements, and Michael Zäch for helpful discussion regarding the AFM data. Partial support was also provided by Biomimetic Materials Science Program funded by the Swedish Foundation for Strategic Research (SSF).

References and Notes

(1) Göpel, W. *Biosens. Bioelectron.* **1998**, *13*, 723.
(2) Collings, A. F.; Caruso, F. *Rep. Prog. Phys.* **1997**, *60*, 65.
(3) Fishman, H. A.; Greenwald, D. R.; Zare, R. N. *Annu. Rev. Biophys. Biomol. Struct.* **1998**, *27*, 165.
(4) Ziegler, C.; Gopel, W. *Curr. Opin. Chem. Biol.* **1998**, *2*, 585.
(5) Niemeyer, C. M.; Blohm, D. *Angew. Chem., Int. Ed.* **1999**, *38*, 2865.
(6) Kasemo, B. *Surf. Sci.* **2002**, *500*, 656−677.
(7) Owens, N. F.; Gingell, D.; Rutter, P. R. *J. Cell Sci.* **1987**, *87*, 667.
(8) O'Connor, S. M.; Gehrke, S. H.; Retzinger, G. S. *Langmuir* **1999**, *15*, 2580.
(9) Chapman, D. *Langmuir* **1993**, *9*, 39.
(10) Malmsten, M. *J. Colloid Interface Sci.* **1994**, *168*, 247.
(11) Sackmann, E. *Science* **1996**, *271*, 43.
(12) Buijs, J.; Britt, D. W.; Hlady, V. *Langmuir* **1998**, *14*, 335.
(13) Pfeiffer, I.; Hook, F. *J. Am. Chem. Soc.* **2004**, *126*, 10224.
(14) Larsson, C.; Wingren, C.; Borrebaeck, C.; Hook, F. *Langmuir*, submitted for publication.
(15) Ferritto, M. S.; Tirrell, D. A. *Macromolecules* **1988**, *21*, 3119.
(16) Ferritto, M. S.; Tirrell, D. A. *Biomaterials* **1990**, *11*, 645.
(17) Martynov, I. Yu.; Demyashkevich, A. B.; Uzhinov, B. M.; Kuz'min, M. G. *Russ. Chem. Rev.* **1977**, *46*, 1.
(18) Pappayee, N.; Mishra, A. K. *Spectrochim. Acta, Part A* **2000**, *56*, 2249.
(19) Mandal, D.; Pal, S. K.; Bhattacharyya, K. *J. Phys. Chem. A* **1998**, *102*, 9710.
(20) Sujatha, J.; Mishra, A. K. J. *Photochem. Photobiol. A: Chem.* **1996**, *101*, 215.
(21) Gutman, M.; Huppert, D.; Pines, E. *J. Am. Chem. Soc.* **1981**, *103*, 3709.
(22) Gutman, M.; Nachiel, E.; Gershon, E.; Giniger, R.; Pines, E. *J. Am. Chem. Soc.* **1983**, *105*, 2210.
(23) Bertran, J.; Chalvet, O.; Daudel, R. *Theor. Chim. Acta* **1969**, *14*, 1.
(24) Soroka, K.; Vithanage, R. S.; Phillips, D. A.; Walker, B.; Dasgupta, P. K. *Anal. Chem.* **1987**, *59*, 629.
(25) Bardez, E.; Chatelain, A.; Larrey, B.; Valeur, B. *J. Phys. Chem.* **1994**, *98*, 2357.
(26) Salamon, Z.; Tollin, G. *Biophys. J.* **2001**, *80*, 1557.
(27) Sauerbrey, G. *Z. Phys.* **1959**, *155*, 206.
(28) Ward, M. D.; Buttry, D. A. *Science* **1990**, *249*, 1000.
(29) Rodahl, M.; Höök, F.; Krozer, A.; Brzezinski, P.; Kasemo, B. *Rev. Sci. Instrum.* **1995**, *66*, 3924.
(30) Thompson, M.; Dhaliwal, G. K.; Arthur, C. L. *Anal. Chem.* **1986**, *58*, 1206.
(31) Muratsugu, M.; Ohta, F.; Miya, Y.; Hosokawa, T.; Kurosawa, S.; Kamo, N.; Ikeda, H. *Anal. Chem.* **1993**, *65*, 2933.
(32) Janshoff, A.; Steinem, C.; Sieber, M.; Galla, H. J. *Eur. Biophys. J. Biophys. Lett.* **1996**, *25*, 105.
(33) Caruso, F.; Furlong, D. N.; Kingshott, P. *J. Colloid Interface Sci.* **1997**, *186*, 129.
(34) Aberl, F.; Wolf, H. Koesslinger, C.; Drost, S.; Woias, P.; Koch, *S. Sens. Actuators, B* **1994**, *18−19*, 271.
(35) Buttry, D. A.; Ward, M. D. *Chem. Rev.* **1992**, *92*, 1355.
(36) Höök, F.; Rodahl, M.; Brzezinski, P.; Kasemo, B. *Langmuir* **1998**, *14*, 729.
(37) Gennis, R. B. *Biomembranes*: *Molecular Structure and Function*; Springer-Verlag: New York, 1989.
(38) Prasad, R., Ed. *Manual on Membrane Lipids*; Springer-Verlag: Berlin, 1996.
(39) MacDonald, R. C.; MacDonald, R. I.; Menco, B. P. M.; Takeshita, K.; Subbarao, N. K.; Hu, L.-R. *Biochim. Biophys. Acta* **1991**, *1061*, 297.
(40) Schneider, J.; Dufréne, Y. F.; Barger, W. R.; Lee, G. U. *Biophys. J.* **2000**, *79*, 1107.
(41) Reimhult, E.; Höök, F.; Kasemo, B. *Langmuir* **2003**, *19*, 1681.
(42) As a side note, 8-hydroxyquinoline can chelate multivalent cations such as Ca^{2+}. Such chelates can result either in cross-links between pairs of 8-hydroxyquinoline ligands bound to a single Ca^{2+} ion or individual metal−ligand moieties with a net charge of +1. However, the uptake of Ca^{2+} by polymers containing 8-hydroxyquinoline was found to take many hours to achieve equilibrium by: Salem N. M.; et al. *React. Funct. Polym.* **2004**, *59*, 63 and Ebraheem, K. A. K.; et al. *Eur. Polym. J.* **1985**, *21*, 97.
(43) Richter, R.; Mukhopadhyay, A.; Brisson, A. *Biophys. J.* **2003**, *85*, 3035.
(44) Zäch, M.; Kasemo, B. *Proc. AIP* **2003**, *CP696*, 447−451.
(45) Keller, C. A.; Kasemo, B. *Biophys. J.* **1998**, *75*, 1397.
(46) Keller, C. A.; Glasmastar, K.; Zhdanov, V. P.; Kasemo, B. *Phys. Rev. Lett.* **2000**, *84*, 5443.
(47) An alternate interpretation for the QCM-D data in Figure 7 is that the bilayer formation is incomplete. The lack of a deep trough in the Δf data is often characteristic of the adsorption of intact vesicles, as is the higher than normal dissipation. However, in this case the lack of a trough results from the high Ca^{2+} concentration (see ref 43). The other reason for discounting the presence of intact vesicles is that none were observed by AFM. Nevertheless, formation of a complete bilayer is not critical for this application.
(48) Berg, H. C. *Random Walks in Biology*; Princeton University Press: Princeton, NJ, 1993; p 42.
(49) Mills, R. *J. Phys. Chem.* **1973**, *77*, 685.
(50) Seki, K.; Tirrell, D. A. *Macromolecules* **1984**, *17*, 1692.
(51) Needham, D.; Mills, J.; Eichenbaum, G. *Faraday Discuss.* **1998**, *111*, 103.

MA048046Q